

Programmable Ultralight Magnets via Orientational Arrangement of Ferromagnetic Nanoparticles within Aerogel Hosts

Yuanyuan Li,[†] Qingkun Liu,[‡] Andrew J. Hess,[‡] Shu Mi,[†] Xiaoduo Liu,[†] Ziyu Chen,[†] Yong Xie,^{*,†,‡,§,||} and Ivan I. Smalyukh^{*,‡,§,||}

[†]School of Physics, Beihang University, Beijing 100191, China

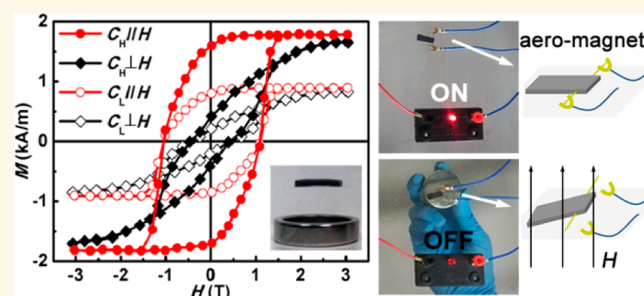
[‡]Department of Physics and Soft Materials Research Center and [§]Materials Science and Engineering Program, Department of Electrical, Computer, and Energy Engineering, University of Colorado, Boulder, Colorado 80309, United States

^{||}Renewable and Sustainable Energy Institute, National Renewable Energy Laboratory and University of Colorado, Boulder, Colorado 80309, United States

Supporting Information

ABSTRACT: The actuation and levitation of air-suspended objects by a magnetic field, due to its noncontact and holonomic manipulation modes, are important technological capabilities for device applications. However, owing to a higher density of conventional ferromagnets or nanoparticle-containing polymers and strong magnetic fields required for actuation, fabricating lightweight materials with a sensitive magnetic response for weight critical applications is challenging. Here, we report ultralight aerogel-based magnets (aero-magnets) comprising assembled ferromagnetic nanomaterials with highly magnetic anisotropy where the magnetic domains can be programmed by external pre-designed fields. To demonstrate the breadth of manufacturing methods for this breed of aero-magnet composites, both silica/nanocellulose aerogel hosts and ferromagnetic nanorod/nanoplatelet guests have been explored. Single and double domains with out-of-plane magnetization are programmed into the aero-magnets and characterized by magnetic force microscopy. The levitation and actuation of the aero-magnets are realized while exposed to a small external magnetic field of 11 mT and introduced to a switching circuit. Furthermore, the elastic moduli of the aero-magnets are estimated by dynamic magnetic responses of the ferromagnetic nanoparticles tightly tethered in the aerogel hosts under rapid cyclic fields. These programmable aero-magnets could serve as monolithic magnetic actuator units in the fields of tiny robots and aerospace components.

KEYWORDS: ultralight magnets, magnetic aerogels, ferromagnetic nanoparticles, self-assembly, programmable magnetic domains



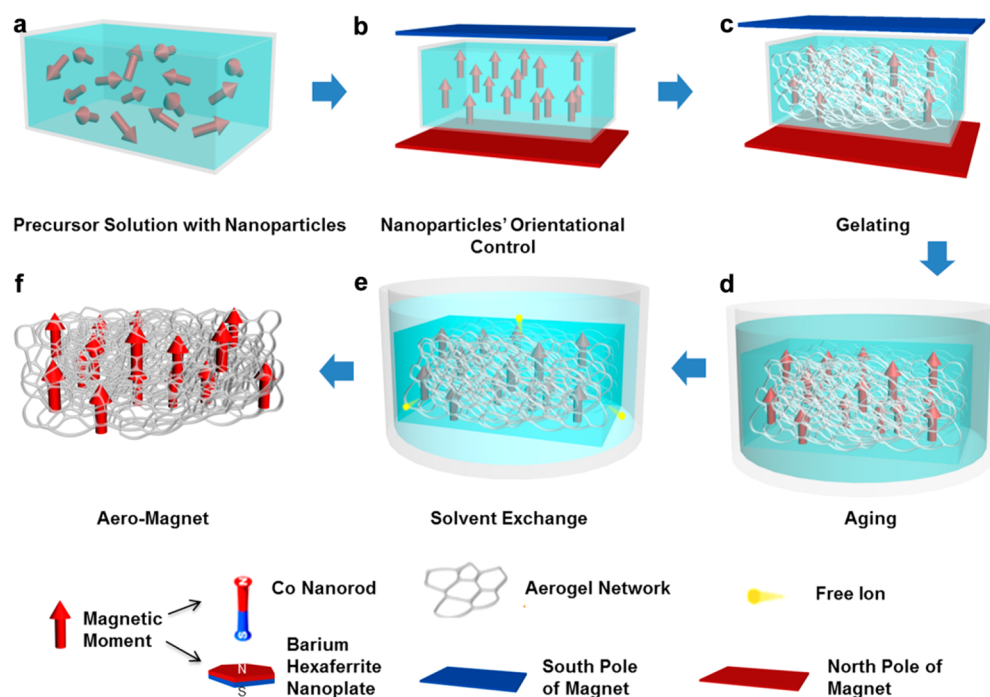
Emerging technologies for smart robots and miniature spacecraft need more lightweight materials and devices with easy manipulability.^{1–4} Existing materials are generally actuated by external stimuli such as optical,^{5–7} electric,^{8,9} or magnetic fields.^{10–12} Magnetic stimulation has advantages of noncontact and remote control, which are applicable in closed or extreme environments.^{13–15} Considerable efforts have been devoted to the development of materials with a sensitive magnetic response. For example, fast-transforming elastomer composites with programmed ferromagnetic domains have been realized by thermoplastic three-dimensional (3D) printing techniques.¹⁶ Nematic liquid crystal doped with orientationally ordered ferromagnetic platelets has shown hysteretic behavior and magnetization reversal in a flipped external field.^{17,18} Hydrogels with coaxially oriented magnetic nanosheets have the ability of directional isolation of

vibrations.¹⁹ However, large densities of these host materials hinder their applications as actuatable units for especially lightweight critical fields. Aerogels, as the lightest solid material which has a density of 0.16 kg m^{-3} in a vacuum,^{20,21} only one-eighth the density of air, are preferred for developing the ultralight composite materials. Additionally, aerogels possess other desirable properties, such as high specific surface areas,^{22,23} low thermal conductivity,^{24,25} and hydrophobicity.²⁶ Aerogel with magnetic nanoparticles, especially ferromagnetic nanoparticles, which combine the advantages of the lightweight and sensitively magnetic response, is a promising candidate for

Received: June 19, 2019

Accepted: December 2, 2019

Published: December 2, 2019

Scheme 1. Procedures for Fabricating Aero-Magnets^a

^a(a) Ferromagnetic nanoparticles are uniformly dispersed in the hydrogel-precursor solution. (b) The ferromagnetic nanoparticles are oriented by a pre-configured, external magnetic field. (c) The solution gels into a hydrogel. (d) The hydrogel is placed in a water bath for aging. (e) The hydrogel is immersed into isopropanol for solvent exchange. (f) The aero-magnet is obtained by critical point drying.

the smart and lightweight applications. Magnetic aerogels had been reported by doping iron or $\text{Nd}_2\text{Fe}_{14}\text{B}$ powders.^{27,28} Flexible aerogels with a high ratio of magnetic nanoparticles in content were also fabricated by using cellulose-based nanofibril as the growth template for the cobalt ferrite nanoparticles.²⁹ To obtain robust magnetic aerogel with high ferromagnetism, we introduce ferromagnetic nanoparticles with large magnetic anisotropy. As a result, the obtained aerogel-based magnets (aero-magnets) have stable ferromagnetic properties because of the tightly tethered and oriented nanoparticles inside the aerogel networks. Moreover, from the view of preparation techniques the magnetically responsive polymers have been realized by the thermoplastic three-dimensional (3D)-printing techniques.^{16,30–32} However, limited by the materials viscosity and printing efficiency, material species are insufficient and the fabricating cost is relatively high.³³ It is also necessary to develop an approach to break through the limitation of materials (such as aerogels and hydrogels) and realize large-area, one-step cast molding of magnetically responsive, lightweight materials at low cost.

In our work, aero-magnets with programmable domains were fabricated by incorporating the dispersed ferromagnetic nanoparticles into aerogel hosts. To demonstrate the generality of the approach, the different ferromagnetic nanoparticles were incorporated within either silica or nanocellulose aerogel hosts. The embedded nanoparticles can be oriented readily along external magnetic fields during the gelation process, thus leading to the magnetic anisotropy and the designable magnetic domains of our aero-magnets. The magnetization of the aero-magnets can be adjusted by changing the doped ratio of the nanoparticles. We also imposed multicycle magnetic fields on the aero-magnets to measure the mechanical responses of the entrapped magnetic nanoparticles and to

reveal the stability and mechanical properties of the nano-composites. Young's modulus was therefore estimated and agreed well with the experimental measurements. Also, a single-domain aero-magnet suspension and a double-domain magnetic-switch were explored for demonstrating the performances concerning noncontact and holonomic manipulation capabilities. The magnetically driven aero-magnets developed here would enable their applications eventually in the fields of emerging lightweight actuators and smart systems.

RESULTS AND DISCUSSION

Our design for aero-magnets is schematically illustrated in Scheme 1. Two kinds of ferromagnetic nanoparticles, Co nanorods and barium hexaferrite nanoplatelets, were employed. The monodispersed Co nanorods with tunable length and width (Table S1 and Figure S1) were synthesized by a polyol method.^{34,35} The barium hexaferrite nanoplatelets with an average lateral size of 140 nm and a thickness of 7 nm were obtained by a hydrothermal method.³⁶ Two different aerogel hosts, silica aerogels and cellulose-based aerogels, were fabricated with their inclusions by a sol-gel process using methyltriethoxysilane as a precursor³⁷ and cross-linking of carboxylated cellulose nanofibers (CNF) in the presence of hydrochloric acid, respectively.³⁸ The procedures for preparation of the aero-magnets were that the ferromagnetic nanoparticles were dispersed in the aerogel precursor solution (Scheme 1a). Then the particles were oriented by imposing localized, uniform fields utilizing a sandwich structure with reversed magnetic poles during the solution state (Scheme 1b). The magnetic field was removed when the sol-gel process was completed with entrapment of the magnetic nanoparticles within the gel (Scheme 1c). The gel was then aged for a specified time (Scheme 1d) and followed by solvent exchange

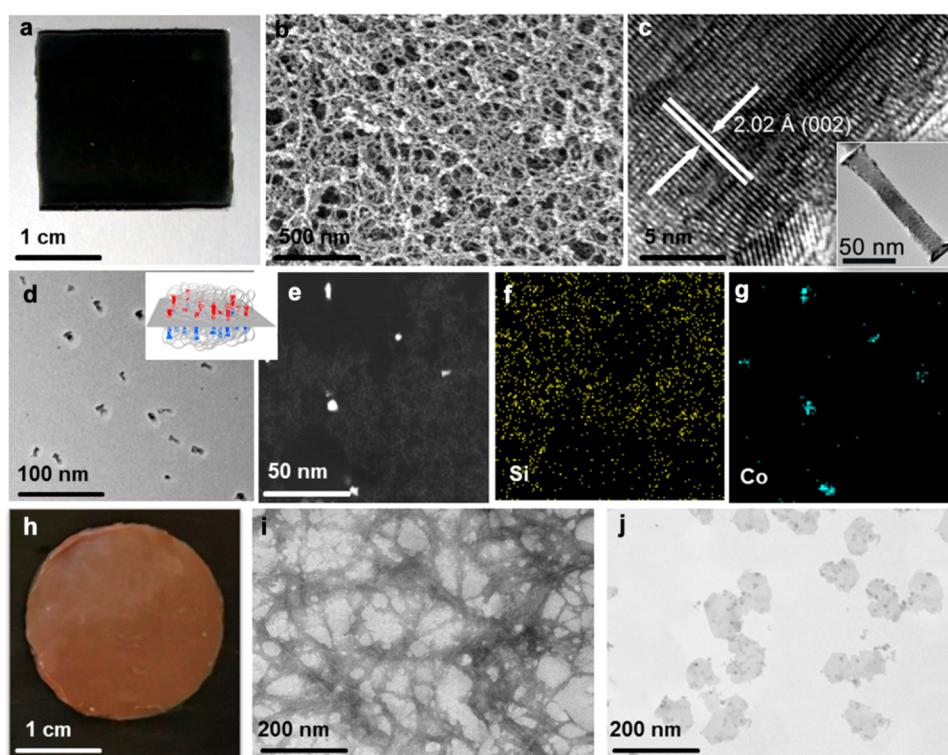


Figure 1. Optical and electronic images of aero-magnets. (a) Optical image of a silica aerogel doped with Co nanorods. (b) SEM image of the surface of the silica aerogel doped with Co nanorods. (c) High-resolution TEM image of a single Co nanorod. The inset is TEM image of an entirety Co nanorod. (d) TEM image of the fault-cutting slice of the aero-magnet showing end-faces of the dispersed nanorods entrapped within the aerogel and orientational alignment of the rods. The inset is a schematic of the fault cutting, where the gray plane represents the direction of fault cutting. (e) Scanning TEM image of the fault-cutting slice. (f,g) Si and Co element mapping, respectively, corresponding to panel e. The discrete yellow points represent the signal of elemental Si in the aerogel whereas the blue spots represent the signal of elemental Co in the nanorods. (h) Optical image of the cellulose-based aerogel doped with barium hexaferrite nanoplatelets. (i) TEM image of the cellulose nanofibers. (j) TEM image of the doped barium hexaferrite nanoplatelets.

with isopropanol (Scheme 1e). At last, aero-magnets were obtained by critical point drying (Scheme 1f). Using the approach, we can obtain samples with a large area, and well-defined shape by a homemade casting mold.

Characterization of Orientation of Anisotropic Nanoparticles within the Aerogels. Inch-scale monolithic aero-magnets with out-of-plane magnetization were fabricated and characterized by optical and electron imaging, exhibiting an aggregation-free dispersion of the magnetic nanoparticles within their mesostructured aerogel host (Figure 1). The silica aero-magnet doped with 30 wt % aligned Co nanorods can be molded into arbitrary shapes in the hydrogel state or be cut into desired shapes after realizing an aerogel form (Figure 1a). The typical aero-magnets have a porosity of about 70% and a density of 0.12 g cm^{-3} , which is only 1.4% that of bulk cobalt. The aero-magnet is comprised of 3D aerogel networks whose constituent fibers have an average diameter of about 10 nm (Figure 1b). The Co nanorods with aspect ratio of ~ 9 are chosen because of their high saturation magnetization ($108 \text{ A}\cdot\text{m}^2/\text{kg}$) and remanence ($50 \text{ A}\cdot\text{m}^2/\text{kg}$) (Figure S2a) which guarantee large magnetization of the aero-magnet at relatively low doping ratio (1800 A/m at 30 wt % doping content) and thus an overall low density for the nanocomposite material. X-ray diffraction data (Figure S2b) indicate no cobalt oxides existed and suggest the reliability of magnetic properties of the aero-magnets. The Co nanorod itself with a diameter of 13 nm and a length of 120 nm on average is a single crystal with a c -axis of (002), which is also the direction of easy magnetization

along the long axis of the nanorods (Figures 1c, S1a, and S2c). The low-energy linear assembly (Figure S2d) further implies that the axial direction is also the direction of the magnetic moment whose orientation is crucial to realize the oriented arrangement of the nanorods in the aerogels along the imposed external field. To obtain the dispersity and orientation information on the nanorods within the aerogels, fault-cut slices were carried out and characterized by scanning TEM (STEM) and element mapping. Well-dispersed nanorods were confirmed to be perpendicular to the cutting plane in the aerogel (Figure 1d and schematic inset). The embedded nanoparticles and background aerogel were identified by the STEM (Figure 1e) and element mapping of Si and Co (Figure 1f,g). Flexible aero-magnets were also fabricated by incorporating barium hexaferrite nanoplatelets with radius-thickness ratio of ~ 20 into a cellulose-based aerogel (Figure 1h). The transmission electron microscopy (TEM) images of the porous CNFs network and dispersed polygonal nanoplatelets are presented in Figure 1i,j.

Compared with the silica-based aero-magnets, the cellulose-based ones possess improved flexibility but degraded ferromagnetism due to the acidic forming environment which etches the magnetic particles despite that we have used silica shells to protect the nanoparticles. In contrast to the nanorods, the nanoplatelets are much harder to maintain the orientational ordering and entire stability owing that the binding ability of nanofibers to the rods is greater than that to the plates. The obtained aero-magnets possess a relatively

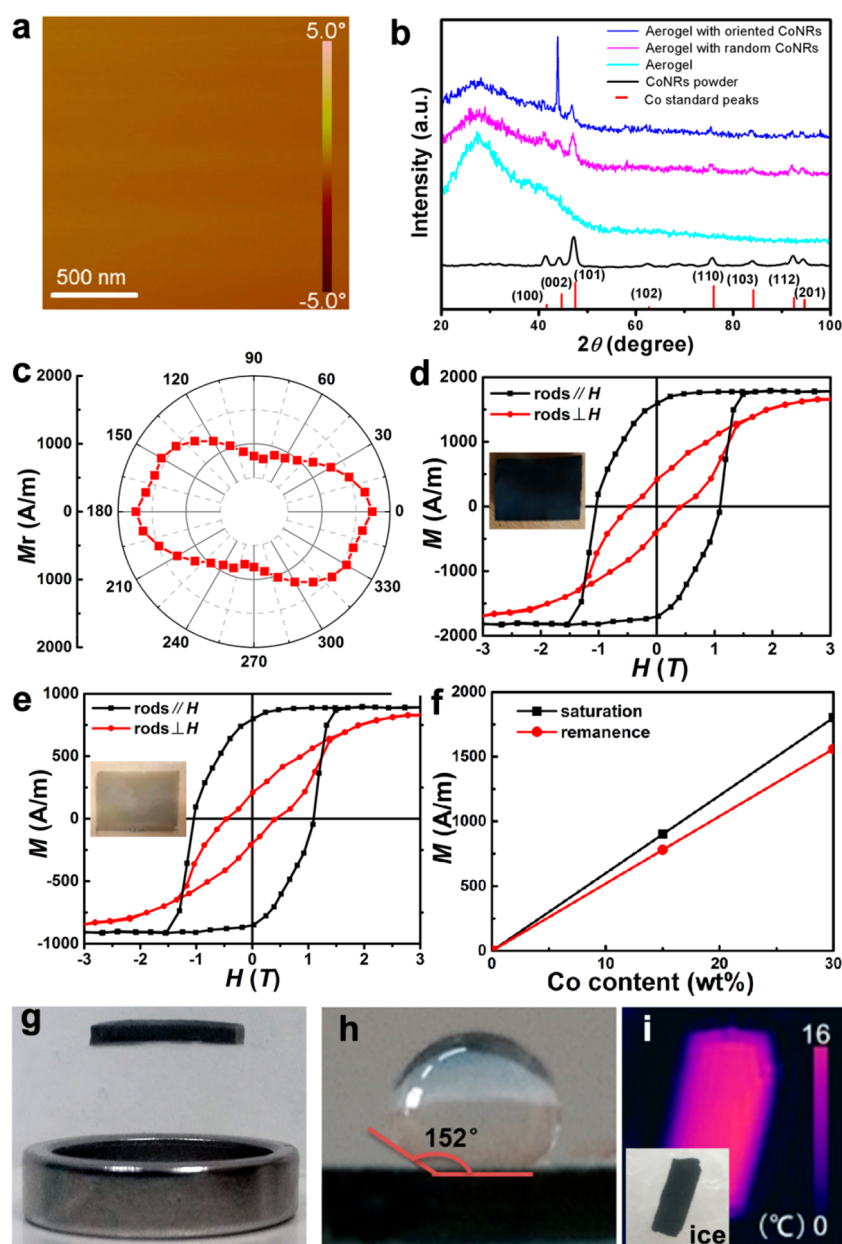


Figure 2. Measurement and adjustment of properties of single-domain aero-magnet. (a) MFM image of the single domain aero-magnet. The color bar represents the phase change (-5° to 5°) caused by the magnetic field from the sample. (b) XRD patterns of the aerogel with oriented Co nanorods, the aerogel with disordered Co nanorods, the pure aerogel, the Co nanorods powders, and the Co standard peaks, where prominent enhancement of diffraction peak of Co (002) plane was obtained. (c) The remanence anisotropy of the single domain aero-magnet with 30% doping content of Co nanorods. (d) The hysteresis loops of the single domain aerogel with 30 wt % Co nanorods at applied fields parallel and perpendicular to the axial direction of Co nanorods, respectively. The inset is the optical image of the measured sample. (e) The hysteresis loops of the single domain aero-magnet with 15 wt % Co nanorods at applied fields parallel and perpendicular to the axial direction of Co nanorods, respectively. The inset is the corresponding optical image of the measured sample. (f) The remanence and saturation magnetization curves with respect to the Co nanorod content where a linear relationship is obtained approximately. (g) Magnetic floating of the aero-magnet with a ring magnet as the base. (h) Hydrophobicity of the aero-magnet. (i) Infrared thermograph of the aero-magnet placed on an ice block showing the thermal insulating property. The inset is the digital photo accordingly.

uniform magnetic field taking into account the homogeneous distribution of the nanoparticles, which are improved in their magnetic properties compared with the conventional magnets whose magnetic field is concentrated on the borders.

Measurement and Adjustment of Magnetic Properties. The obtained aero-magnets have prominent ferromagnetic properties which can be observed by an applied external field or measured by vibration sample magnetometer (VSM) and tuned by the content of the guest ferromagnetic

nanoparticles. We illustrated the adjustment ability by using silica-based aerogel with Co nanorods as an example. Dynamic responses of a single domain aero-magnet under a flipped magnetic field (Movie S1) demonstrate the effective control over the orientation of the magnetization of the aero-magnet. Owing to the designed magnetic field perpendicular to the sample's plane, the aero-magnet appears to have repulsive or attractive responses while applying the opposite or the same field. To match the compatibility of the targeted applications in

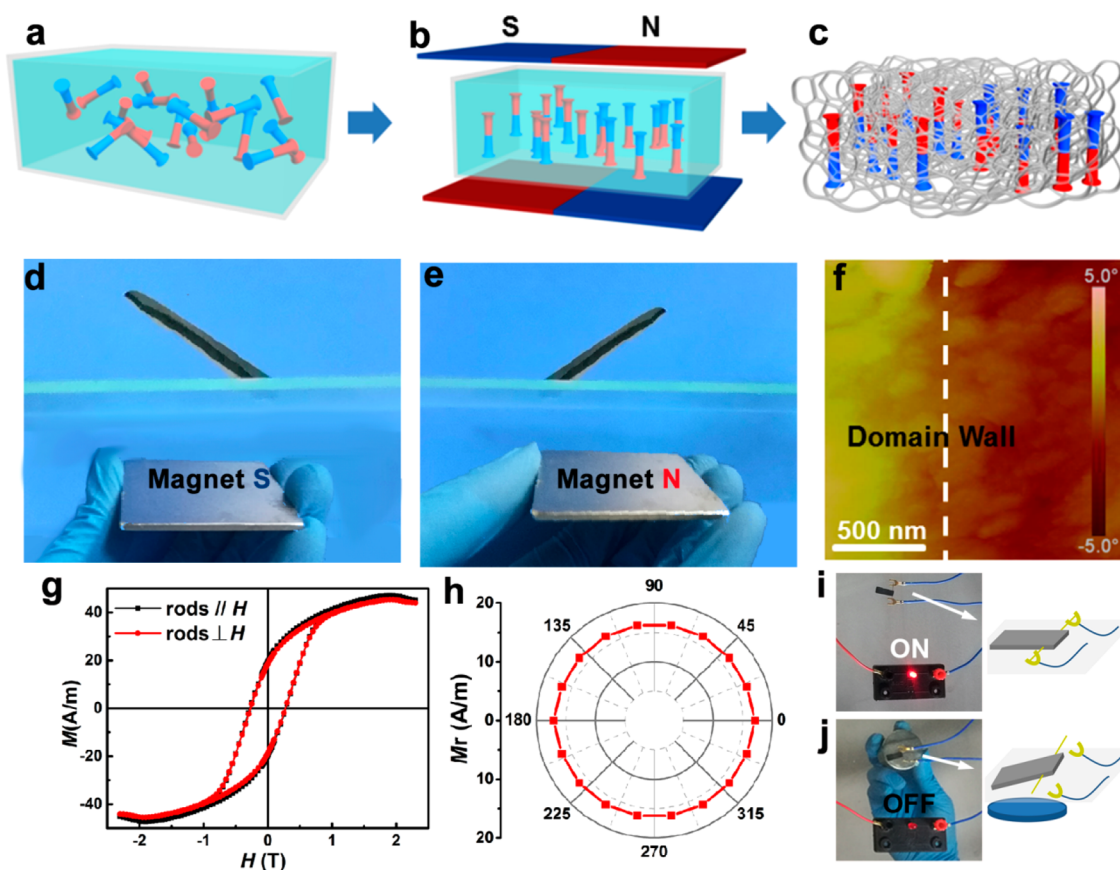


Figure 3. Design and measurement of magnetic properties of double domain aero-magnet. (a–c) Schematics illustrating the fabricating processes of the double domain aero-magnets. (d,e) The dynamic responses of the aero-magnet under two opposing magnetic polarities, respectively. (f) MFM image of the aero-magnet, where a clear domain wall is distinguished at the border of the two domains. The color bar represents the phase change (-5° to 5°) caused by the magnetic field from the sample. (g) The hysteresis loops of the aero-magnet at applied fields parallel and perpendicular to the axial direction of Co nanorods, respectively. (h) The angular dependence of remanence of the double domain aero-magnet. (i,j) The magnetic switch unit realized on a circuit loop and the on/off effects exhibited by using the double-domain aero-magnet as the switch. The right insets schematically show the design of the magnetic switch with a fine copper wire penetrating through the aero-magnet as the contact electrode.

lightweight critical fields, a small permanent magnet with side length of 1 cm is applied and by far enough to actuate the obtained aero-magnet as presented in the movie. The zone of the single domain was further probed by magnetic force microscopy (MFM), which indicates a uniform dispersion and orientation of the Co nanorods within the aerogel (Figure 2a). To give more evidence on a relatively large scale, X-ray diffraction (XRD) patterns (Figure 2b) were performed to examine the consistent orientation of the Co nanorods within the aerogel. A broad diffraction peak around 30° was exhibited first by measuring the pure aerogel, which was associated with amorphous silica. After doping of random Co nanorods, obvious crystal diffraction peaks of hexagonal Co were obtained, which match well with the standard peaks of Co powders. In comparison, the aerogel with oriented Co nanorods has a greatly enhanced peak of (002) plane at 44.7° , consistent with the orderly arrangement of the nanorods with their long axis perpendicular to the aerogel's plane, indicating the overall uniform orientation of the Co nanorods in the aerogel. Out-of-plane magnetic anisotropy of the aero-magnets further shows the easy direction of magnetization along the axial direction of rods (Figure 2c). Moreover, two aero-magnets doped with 30 and 15 wt % of the Co nanorods, respectively, exhibited different saturation magnetizations and

remanences, proportional roughly to the doping content of the nanorods (Figure 2d–f). The insets in Figure 2d,e show further the transparency increase with the reduction of the nanorods' doping content. Interestingly, floating of the aero-magnet was also realized by subtly tuning the distance and balance point of the sample from a ring magnet with strength of about 11 mT at the suspending position along the symmetry axis (Figure 2g), combining the good hydrophobicity (contact angle $\sim 152^{\circ}$) and low thermal conductivity of the aero-magnet (Figure 2h,i), suggesting the promising applications in lightweight, actuable units.

Programmability of Magnetic Domains. To demonstrate the diversity of our design, an aero-magnet with two adjacent domains containing opposite magnetization vector was obtained. The preparation processes are illustrated schematically in Figure 3a–c, where two opposite fields were imposed on the sample during the gelation process (Figure 3b). Owing to this double-domain design, the aero-magnet keeps always an inclined angle with an applied external field and transfers to the mirroring angle when reversing the field's polarity, as shown in Figure 3d,e and Movie S2. Direct evidence of the double-domain composition was also obtained by the MFM imaging (Figure 3f) wherein a domain wall appeared at the interface of the two domains. Slight difference

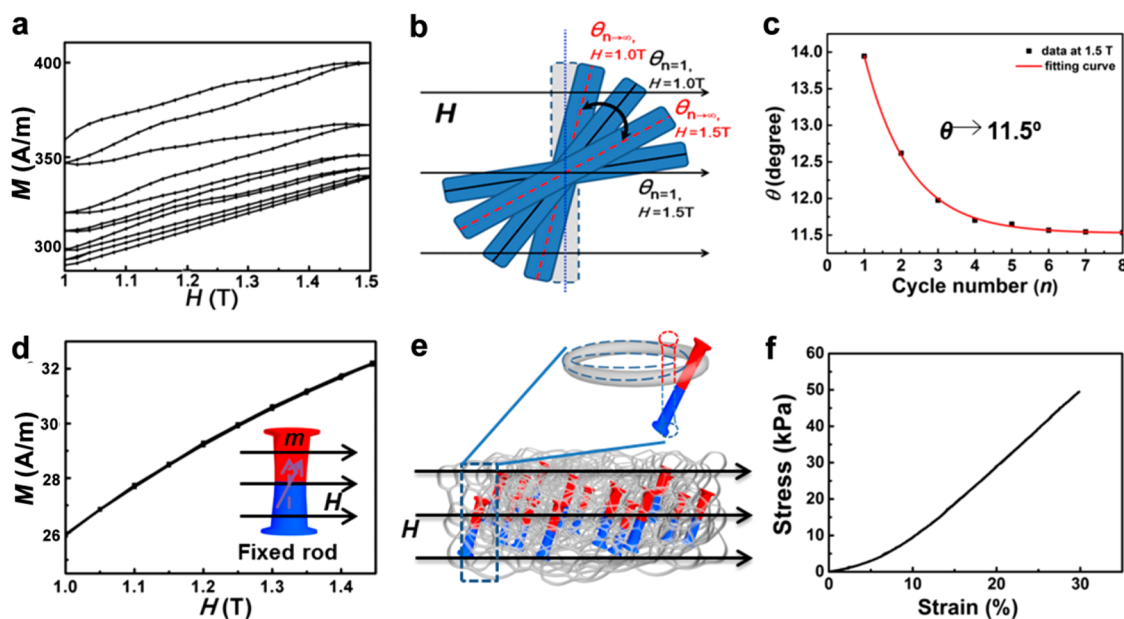


Figure 4. Dynamic response of aero-magnet under a fast cyclic field and evaluation of the elastic modulus. (a) The magnetization curves of the aero-magnet under multicycle fields varied from 1 to 1.5 T. (b) An illustration showing the dynamic responses of Co nanorods within the aerogel networks under the cycled fields. (c) The experimental data and fitting curve of rotation angles of the Co nanorods with respect to the number of cycles under the terminated field of 1.5 T, corresponding to the panel a. (d) The magnetization curves of a magnetic gel with fixed Co nanorods, indicating the variation of magnetic moment with the outer field through eight times cycle. No damping of magnetization was found. (e) The schematic of rotation of Co nanorods with the applied magnetic field. The upper-right part shows the stretching of the aerogel network by the Co nanorod due to the magnetic interaction. (f) Stress–strain curve of the aero-magnet for measuring Young’s modulus.

in hysteresis loops and remanence anisotropy indicates a minor magnetic anisotropy in the aero-magnet due to the compensating effect of the symmetric inverse domains (Figure 3g,h). The magnetic responses of the aero-magnet allow us to implement a trial exploration in, for example, magnetic switch. The double-domain aerogel with which a thin copper wire penetrated its one end as the contact electrode was therefore introduced into a circuit loop as shown in Figure 3i,j. By applying a magnetic field from the circuit periphery, such as the bottom in our experiments, the aero-magnet was lifted up and then fell back following the removal of the magnetic field, leading to the turn-off and turn-on of the circuit accordingly (Movie S3). Besides, beyond the single and double domains, multidomain aero-magnets could be designed using our simple sol–gel approaches. Additionally, hydrogels with orientational magnetic dipoles (Scheme 1a–d) had also been realized in our experiments (Movie S4), whereas our hydrogels should have better flexibility and biocompatibility than the aerogels have.

Evaluation of Stability and Elastic Properties. To examine the stability of aero-magnet and the interactions between the particles and the aerogel network, we used a fast oscillating field varying from 1 to 1.5 T to detect the variation of magnetization intensity (M). A damped swing effect of the aero-magnet’s magnetization was found (Figure 4a), which should be attributed to the damped oscillation of Co nanorods driven by a magnetic field in the aerogel host. As the magnetic field rapidly reached 1 T, the magnetic torque applied to the Co nanorods leads to an oscillation of the nanorods with an initial angular velocity at the angle of $\theta_{n=1, H=1\text{ T}}$ in their aerogel matrix (Figure 4b), where n denotes the number of cycles. With the continued increase of the field, the nanorods reached the angle of $\theta_{n=1, H=1.5\text{ T}}$. This kinetic process reaches an equilibrium state due to the damping force after several cycles

of the applied magnetic field and results in a final stable magnetization value of the aero-magnet. The nanorods then swing between two constant positions, $\theta_{n \rightarrow \infty, H=1\text{ T}}$ and $\theta_{n \rightarrow \infty, H=1.5\text{ T}}$. This damping effect allows us to find the nanorods’ equilibrium angle associated with the competition between the magnetic and elastic torques acting on the Co nanorods constrained in an aerogel’s skeleton. Measurement uncertainty of the oscillating field can be estimated by rotating the aero-magnet (10° or -10°) with respect to the direction of external field used for the collection of magnetization-magnitude data (Figure S3). Then we fit the swing angle of the nanorods at 1.5 T as a function of the number of cycles n using a damping formula. A constant rotation angle of $\theta \rightarrow 11.5^\circ$ is obtained when $n \rightarrow \infty$ (Figure 4c, Table S2, and Figure S4), which supplies quantifiable strain of the aero-magnet network under the action of the applied field. To clarify the origin of the damping of M , which could be attributed to either a rotation of the magnetic moment or rotation of the rods, a contrast experiment was carried out using ethyl acrylate adhesive to replace the aerogels and to mechanically constrain the movement of Co nanorods. In such a case, no damping of M was observed (Figure 4d), indicating that the damping did come from the swinging of the nanorods rather than rotation of the magnetic moment. Figure 4e schematically displays that the rotation of Co nanorods stretches the aerogel network, damps their rotational oscillations, and consumes the initial rotational kinetic energy obtained from the initial ramping of $H = 0$ to 1 T. By these analyses, we conclude that the aero-magnet can be stable even under the action of a strong magnetic field.

The Young’s modulus of the aero-magnet was further estimated according to the above results (Figure S5). The magnetic torque (L_m) from the field should equal to the elastic

torque (L_e) from the aerogel when $n \rightarrow \infty$. The magnetic torque can be written as

$$L_m = H\mu_0 m v \cos \theta \quad (1)$$

where H is the magnetic field strength, μ_0 is the permeability of vacuum, m is moment per unit volume, v is the volume occupied by Co nanorod, and θ is rotation angle of Co nanorods.

The elastic torque can be obtained by integrating the torques on the nanorods

$$L_e = ES l \quad (2)$$

where E is Young's modulus, S is the contact area which is half of a rod's lateral surface area, and l is the half-length of the rod. When $L_m = L_e$, Young's modulus is given as follows

$$E = \frac{H\mu_0 m v \cos \theta}{S l} \quad (3)$$

Utilizing the fitted result from Figure 4c, Young's modulus of the aero-magnet was given to be 181 ± 24 kPa, which agreed well with the experimental measurements of 164 kPa (Figure 4f). Shear modulus of the aero-magnet was further determined to be 74 kPa (eq S5) with Poisson's ratio of about 0.22.³⁹

CONCLUSION

In summary, we achieved ultralight, programmable aero-magnets with magnetic anisotropy by embedding orientationally ordered, ferromagnetic nanoparticles into aerogels. The obtained aero-magnets possess high magnetization and remanence tuned linear-approximately by the doping ratio of the ferromagnetic nanoparticles. The programmability of the magnetic domains gives the aero-magnets diverse magnetic responses with which we realize the exhibitions of the magnetic levitation and magnetic switch. The stability of the nanocomposite was verified and the mechanical moduli were estimated by analyses of the interactions between the Co nanorods and the aerogel networks. The strategy developed here could give the inspiration for exploring multifunctionalized, lightweight, aerogel-based magnetic materials with different ferromagnetic nanoparticles and aerogel matrixes, which are still ongoing in our lab. The lightweight aero-magnets could be of interest to many potential applications in the fields of the monolithic magnetic actuator, soft robots, spacecraft, and so forth.

METHODS

Synthesis of Co Nanorods.^{34,35} The Co nanorods were synthesized by a polyol method. First, the cobalt(II) carboxylates, $\text{Co}(\text{C}_n\text{H}_{2n+1}\text{COO})_2$ ($n = 7, 9, 11$), were prepared by the reaction of CoCl_2 (5.0 g) and sodium laurate (8.35 g) at 60 °C. The precipitate was washed three times with methanol and then dried in a desiccator. Then cobalt laurate (2.73 g), RuCl_3 (0.039 g), and NaOH (0.225 g) were added to 75 mL of diethylene glycol. The mixture was heated to 170 °C and maintained for 15 min with mechanical stirring. After cooling to room temperature, the black powder was recovered by centrifugation at 8500 rpm for 15 min, washed thrice with ethanol, and finally dried in an oven at 50 °C.

Synthesis of Barium Hexaferrite Nanoplatelets.³⁶ Barium hexaferrite $\text{BaCr}_{0.5}\text{Fe}_{11.5}\text{O}_{19}$ nanoplatelets were synthesized by the hydrothermal method. Typically, 0.01 mol L^{-1} of $\text{Ba}(\text{NO}_3)_2$, 0.045 mol L^{-1} of $\text{Fe}(\text{NO}_3)_3$, and 0.005 mol L^{-1} of $\text{Cr}(\text{NO}_3)_3$ were dissolved in deionized water and coprecipitated by 2.72 mol L^{-1} of NaOH aqueous solution in a Teflon-lined autoclave. The solution was heated to 220 °C and maintained for 1 h and then cooled down to room

temperature. The precipitate was washed with 10 wt % nitric acid and acetone and then redispersed in 1 mL of water.

Preparation of Aero-Magnets. For a silica aerogel³⁷ doped with Co nanorods, 500 μL of methyltriethoxysilane was added to 1 mL of 5 mol L^{-1} HNO_3 solution under stirring for 30 min. Then, 1 mL of polyoxyethylene octyl phenyl ether (Triton X-100) was added into the dispersion while stirring for 5 min. An ice bath was applied for 5 min and followed by adding 1 mL of tetramethylammonium hydroxide with the expected amount of Co nanorods while stirring for 1 min. The reaction mixture was then degassed in a vacuum oven and transferred into a mold with a diameter of 5 cm, sealed for gelation, and allowed to age for 3 days in an 80 °C furnace. The hydrogel was taken from the mold, immersed in deionized water for 24 h, and subsequently followed by solvent exchange with isopropanol, which was replaced by clean isopropanol every 12 h at room temperature for 2 days. Finally, CO_2 supercritical drying at 38 °C under 8.6 MPa was conducted to obtain the dried aerogel samples in a critical point dryer.

For cellulose-based aerogels³⁸ doped with barium hexaferrite nanoplatelets, 1 vol % of aqueous CNFs and an expected amount of barium hexaferrite nanoplatelets were mixed under stirring, followed by several drops of 1 mol L^{-1} of hydrochloric acid solution, which prompts the formation of a hydrogel. The dispersion was poured into a mold and kept at room temperature for 2 h. Then, the hydrogel was immersed in isopropanol for 2 days as a solvent exchange. Finally, the ensuing organogel was put into heptane at 90 °C for 12 h. The heptane, having extremely low surface tension, did not collapse the gel's solid network as the heptane evaporated.

Characterizations. The morphology of samples was characterized by scanning electron microscope (Hitachi, S-4800) and transmission electron microscope (TEM) (JEOL, JEM-2100). Magnetic force microscopy images were obtained on a scanning probe microscope with a magnetic probe (Veeco, Dimension 3100). Magnetic measurements were recorded by a vibration sample meter (Lakeshore 7400). Young's modulus was measured by a texture analyzer (Ensoul, TMS-PRO) with a detection probe of 1 cm at a speed of 0.2 mm min^{-1} . Infrared thermography was collected by an infrared camera (Flir, one pro) on an ice cube. X-ray diffraction was collected on a diffractometer (Rigaku, D/MAX-2500) with a Cu K- α wavelength X-ray source. Fault cutting was obtained by an ultramicrotome for ultrathin sectioning (Leica, EM UC6) with a 50 nm thickness for each slice. High-resolution TEM and element mapping were recorded by a field-emission high-resolution transmission electron microscope (FEI, Tecnai G2 F30) with an accelerator voltage of 300 kV.

ASSOCIATED CONTENT

Supporting Information

The Supporting Information is available free of charge at <https://pubs.acs.org/doi/10.1021/acsnano.9b04818>.

Magnetic response of single domain aero-magnet under a reversing field (MP4)

Magnetic response of the designed double domain aero-magnet (MP4)

Switch-on and -off of the circuit controlled by a double-domain aero-magnet (MP4)

Magnetic response of single domain hydrogel (MP4)

Figures and tables showing the adjustment and characterization of synthesized Co nanorods, magnetization of the aero-magnet with single domain for uncertainty evaluation, the fitting process of damped oscillating rods, and calculation of Young's modulus (PDF)

AUTHOR INFORMATION

Corresponding Authors

*E-mail: xiey@buaa.edu.cn.

*E-mail: ivan.smalyukh@colorado.edu.

ORCID

Yong Xie: 0000-0003-3574-2883

Ivan I. Smalyukh: 0000-0003-3444-1966

Author Contributions

Y.L., Y.X., and Q.L. conceived the idea, designed the study, and interpreted the results. S.M. performed MFM measurements and interpreted the results. Y.X. drafted the manuscript with inputs from all other authors. A.J.H., X.L., Z.C., and I.I.S. modified the manuscript. Y.X. and I.I.S. supervised the study.

Notes

The authors declare no competing financial interest.

ACKNOWLEDGMENTS

This work was supported by the Fundamental Research Funds for the Central Universities (No. YWF-19-BJ-J-211) and National Natural Science Foundation of China (No. 51502011, 11774018, 11904195) and the Beijing Key Discipline Foundation of Condensed Matter Physics. The aerogel development research at the University of Colorado was supported by the U.S. Department of Energy, ARPA-E award DE-AR0000743.

REFERENCES

- (1) Bauer, S.; Bauer-Gogonea, S.; Graz, I.; Kaltenbrunner, M.; Keplinger, C.; Schwodiauer, R. 25th Anniversary Article: A Soft Future: From Robots and Sensor Skin to Energy Harvesters. *Adv. Mater.* **2014**, *26*, 149–162.
- (2) Ma, K. Y.; Chirarattananon, P.; Fuller, S. B.; Wood, R. J. Controlled Flight of aBiologically Inspired, Insect-Scale Robot. *Science* **2013**, *340*, 603–607.
- (3) Levchenko, I.; Keidar, M.; Cantrell, J.; Wu, Y. L.; Kuninaka, H.; Bazaka, K.; Xu, S. Explore Space Using Swarms of Tiny Satellites. *Nature* **2018**, *562*, 185–187.
- (4) Jones, S. M. Aerogel: Space Exploration Applications. *J. Sol-Gel Sci. Technol.* **2006**, *40*, 351–357.
- (5) Zeng, H.; Wasylczyk, P.; Parmeggiani, C.; Martella, D.; Burrelli, M.; Wiersma, D. S. Light-Fueled Microscopic Walkers. *Adv. Mater.* **2015**, *27*, 3883–3887.
- (6) Nocentini, S.; Parmeggiani, C.; Martella, D.; Wiersma, D. S. Optically Driven Soft Micro Robotics. *Adv. Opt. Mater.* **2018**, *6*, 1800207.
- (7) Park, S. J.; Gazzola, M.; Park, K. S.; Park, S.; Santo, V. D.; Blevins, E. L.; Lind, J. U.; Campbell, P. H.; Dauth, S.; Capulli, A. K.; Pasqualini, F. S.; Ahn, S.; Cho, A.; Yuan, H.; Maoz, B. M.; Vijaykuma, R.; Choi, J. W.; Deisseroth, K.; Lauder, G. V.; Mahadevan, L.; et al. Phototactic Guidance of aTissue-Engineered Soft-Robotic Ray. *Science* **2016**, *353*, 158–162.
- (8) Migliorini, L.; Santaniello, T.; Yan, Y.; Lenardi, C.; Milani, P. Low-Voltage Electrically Driven Homeostatic Hydrogel-Based Actuators for Underwater Soft Robotics. *Sens. Actuators, B* **2016**, *228*, 758–766.
- (9) Amjadi, M.; Sitti, M. High-Performance Multiresponsive Paper Actuators. *ACS Nano* **2016**, *10*, 10202–10210.
- (10) Klumpp, S.; Lefevre, C. T.; Bennet, M.; Faivre, D. Swimming with Magnets: From Biological Organisms to Synthetic Devices. *Phys. Rep.* **2019**, *789*, 1–54.
- (11) Poddar, S.; Sa, P. D.; Cai, R.; Delannay, L.; Nysten, B.; Piroux, L.; Jonas, A. M. Room-Temperature Magnetic Switching of the Electric Polarization in Ferroelectric Nanopillars. *ACS Nano* **2018**, *12*, 576–584.
- (12) Lum, G. Z.; Ye, Z.; Dong, X.; Marvi, H.; Erin, O.; Hu, W.; Sitti, M. Shape-Programmable Magnetic Soft Matter. *Proc. Natl. Acad. Sci. U. S. A.* **2016**, *113*, E6007–E6015.

(13) Rahmer, J.; Stehning, C.; Gleich, B. Spatially Selective Remote Magnetic Actuation of Identical Helical Micromachines. *Sci. Robot.* **2017**, *2*, No. eaal2845.

(14) Martel, S. BeyondImaging: Macro- and Microscale Medical Robots Actuated by Clinical MRI Scanners. *Sci. Robot.* **2017**, *2*, No. eaam8119.

(15) Cabrera, D.; Coene, A.; Leliaert, J.; Artes-Ibanez, E. J.; Dupre, L.; Telling, N. D.; Teran, F. J. Dynamical Magnetic Response of Iron Oxide Nano Articles Inside Live Cells. *ACS Nano* **2018**, *12*, 2741–2752.

(16) Kim, Y.; Yuk, H.; Zhao, R.; Chester, S. A.; Zhao, X. Printing Ferromagnetic Domains for Untethered Fast-Transforming Soft Materials. *Nature* **2018**, *558*, 274–279.

(17) Mertelj, A.; Lisjak, D.; Drogenik, M.; Copic, M. Ferromagnetism in Suspensions of Magnetic Platelets in Liquid Crystal. *Nature* **2013**, *504*, 237–241.

(18) Hess, A. J.; Liu, Q.; Smalyukh, I. I. Optical Patterning of Magnetic Domains and Defects in Ferromagnetic Liquid Crystal Colloids. *Appl. Phys. Lett.* **2015**, *107*, 071906.

(19) Liu, M.; Ishida, Y.; Ebina, Y.; Sasaki, T.; Hikima, T.; Takata, M.; Aida, T. An Anisotropic Hydrogel with Electrostatic Repulsion between Cofacially Aligned Nanosheets. *Nature* **2015**, *517*, 68–72.

(20) Si, Y.; Yu, J.; Tang, X.; Ge, J.; Ding, B. Ultralight Nanofibre-Assembled Cellular Aerogels with Superelasticity and Multifunctionality. *Nat. Commun.* **2014**, *5*, 5802.

(21) Sun, H.; Xu, Z.; Gao, C. Multifunctional, Ultra-Flyweight, Synergistically Assembled Carbon Aerogels. *Adv. Mater.* **2013**, *25*, 2554–2560.

(22) Barrios, E.; Fox, D.; Sip, Y. Y. L.; Catarata, R.; Calderon, J. E.; Azim, N.; Afrin, S.; Zhang, Z.; Zhai, L. Nanomaterials in Advanced, High-Performance Aerogel Composites: A Review. *Polymers* **2019**, *11*, 726.

(23) Bheekun, N.; Abu Talib, A. R.; Hassan, M. R. Aerogels in Aerospace: An Overview. *Adv. Mater. Sci. Eng.* **2013**, *2013*, 1.

(24) Xu, X.; Zhang, Q.; Hao, M.; Hu, Y.; Lin, Z.; Peng, L.; Wang, T.; Ren, X.; Wang, C.; Zhao, Z.; Wan, C.; Fei, H.; Wang, L.; Zhu, J.; Sun, H.; Chen, W.; Du, T.; Deng, B.; Cheng, G. J.; Shakir, I.; et al. Double-Negative-Index Ceramic Aerogels for Thermal Superinsulation. *Science* **2019**, *363*, 723–727.

(25) Wang, H.; Zhang, X.; Wang, N.; Li, Y.; Feng, X.; Huang, Y.; Zhao, C.; Liu, Z.; Fang, M.; Ou, G.; Gao, H.; Li, X.; Wu, H. Ultralight, Scalable, and High-Temperature-Resilient Ceramic Nanofiber Sponges. *Sci. Adv.* **2017**, *3*, No. e1603170.

(26) Malfait, W. J.; Juranyi, F.; Zhao, S.; Arreguin, S. A.; Koebel, M. M. Dynamics of Silica Aerogel's Hydrophobic Groups: A Quasielastic Neutron Scattering Study. *J. Phys. Chem. C* **2017**, *121*, 20335–20344.

(27) Leventis, N.; Elder, I. A.; Long, G. J.; Rolison, D. R. Using Nanoscopic Hosts, Magnetic Guests, and Field Alignment to Create Anisotropic Composite Gels and Aerogels. *Nano Lett.* **2002**, *2*, 63–67.

(28) Gich, M.; Casas, L.; Roig, A.; Molins, E.; Sort, J.; Surinach, S.; Baro, M. D.; Munoz, J. S.; Morellon, L.; Ibarra, M. R.; Nogues, J. High-Coercivity Ultralight Transparent Magnets. *Appl. Phys. Lett.* **2003**, *82*, 4307–4309.

(29) Olsson, R. T.; Samir, M. A. S. A.; Salazar-Alvarez, G.; Belova, L.; Strom, V.; Berglund, L. A.; Ikkala, O.; Nogues, J.; Gedde, U. W. Making Flexible Magnetic Aerogels and Stiff Magnetic Nanopaper Using Cellulose Nanofibrils as Templates. *Nat. Nanotechnol.* **2010**, *5*, 584–588.

(30) Bollig, L. M.; Hilpisch, P. J.; Mowry, G. S.; Nelson-Cheeseman, B. B. 3D Printed Magnetic Polymer Composite Transformers. *J. Magn. Magn. Mater.* **2017**, *442*, 97–101.

(31) Huber, C.; Abert, C.; Bruckner, F.; Groenefeld, M.; Muthsam, O.; Schuschnigg, S.; Sirak, K.; Thanhoffer, R.; Teliban, I.; Vogler, C.; Windl, R.; Suess, D. 3D Print of Polymer Bonded Rare-Earth Magnets, and 3D Magnetic Field Scanning with an End-User 3D Printer. *Appl. Phys. Lett.* **2016**, *109*, 162401.

(32) Truby, R. L.; Lewis, J. A. Printing Soft Matter in Three Dimensions. *Nature* **2016**, *540*, 371–378.

(33) Wu, P.; Wang, J.; Wang, X. A Critical Review of the Use of 3-D Printing in the Construction Industry. *Autom. Constr.* **2016**, *68*, 21–31.

(34) Soumare, Y.; Garcia, C.; Maurer, T.; Chaboussant, G.; Ott, F.; Fievet, F.; Piquemal, J. Y.; Viau, G. Kinetically Controlled Synthesis of Hexagonally Close-Packed Cobalt Nanorods with High Magnetic Coercivity. *Adv. Funct. Mater.* **2009**, *19*, 1971–1977.

(35) Bao, L.; Low, W. L.; Jiang, J.; Ying, J. Y. Colloidal Synthesis of Magnetic Nanorods with Tunable Aspect Ratios. *J. Mater. Chem.* **2012**, *22*, 7117–7120.

(36) Liu, Q.; Ackerman, P. J.; Lubensky, T. C.; Smalyukh, I. I. Biaxial Ferromagnetic Liquid Crystal Colloids. *Proc. Natl. Acad. Sci. U. S. A.* **2016**, *113*, 10479–10484.

(37) Liu, Q.; Frazier, A. W.; Zhao, X.; De La Cruz, J. A.; Hess, A. J.; Yang, R.; Smalyukh, I. I. Flexible Transparent Aerogels as Window Retrofitting Films and Optical Elements with Tunable Birefringence. *Nano Energy* **2018**, *48*, 266–274.

(38) Liu, Q.; Smalyukh, I. I. Liquid Crystalline Cellulose-Based Nematogels. *Sci. Adv.* **2017**, *3*, No. e1700981.

(39) Gross, J.; Reichenauer, G.; Fricke, J. Mechanical Properties of SiO₂ Aerogels. *J. Phys. D: Appl. Phys.* **1988**, *21*, 1447–1451.